Simulations of doped CeO_2 at finite dopant concentrations

John A. Purton[a], Neil L. Allan[b] and David S.D. Gunn[a]

[a] Scientific Computing Department, STFC, Daresbury Laboratory, Keckwick Lane, Warrington, WA4 4AD, U.K.

[b] School of Chemistry, Cantock's Close, University of Bristol, Bristol, BS8 1TS

ABSTRACT:

Monte Carlo calculations are reported of calcium- and gadolinium-doped ceria solid solutions, $Ce_{1-x}Ca_xO_{2-x}$ (CDC) and $Ce_{1-x}Gd_xO_{2-x/2}$ (GDC) as a function of dopant concentration x. Previous work has largely been restricted to the dilute defect limit, made a priori assumptions of the formation of particular clusters, and neglected temperature effects. All these constraints are removed in our study. We examine and compare the formation of Ca and Gd-nanodomains with increasing dopant concentration. The growth of Ca-rich domains in $Ce_{1-x}Ca_xO_{2-x}$ is particularly marked even at low concentrations of calcium.
Conductivities of the configurations generated in the Monte Carlo simulations are calculated using molecular dynamics. The Monte Carlo generates the thermodynamically most stable low-energy atomic arrangements and these configurations possess low conductivities relative to those in which the dopants are distributed at random; the nanodomains formed by the dopants reduce oxygen mobility due to the low local concentration of oxygen vacancies and the blocking of pathways for vacancy migration. The calculated conductivity of a $\Sigma5(310)$ grain boundary of $Ce_{1-x}Gd_xO_{2-x/2}$ with overall composition $x = 0.2$ is comparable to that of the bulk material despite pronounced segregation to the interfacial region.
Overall our results illustrate the importance of kinetic vs. thermodynamic control in synthesis of these systems.

1 INTRODUCTION

Doped ceria is receiving intense current attention in particular as an electrolyte for solid oxide fuel cells (SOFCs) at intermediate temperatures.[1,2,3]. Most of this work, both experimental and computational[4], has concentrated on rare-earth dopants such as gadolinium, since the ionic conductivity can be enhanced by the oxygen vacancies generated by the incorporation of a cation with a charge lower than that of Ce. For example experiment[1] shows the conductivity of gadolinium-doped ceria ($Gd_xCeO_{2-x/2}$) passes through a maximum between 10-20% Gd^{3+}. Conductivities also vary with sample thermal history[5]. For compositions $x \geq 0.2$ a marked decrease in conductivity was observed for the aged samples and this was attributed to the formation of micro-domains.[5] Grain boundaries also complicate the problem, as they contribute to dc conductivities and optimisation of the microstructure is required to produce an optimum electrolyte.

The variation of the conductivity with dopant concentration has long been explained in terms of interactions between dopant and anion vacancies and the formation of associated clusters with increasing concentration. In $Ce_{1-x}Gd_xO_{2-x/2}$ (GDC), for example, extended defects are thought to be present locally[6] such that solid solutions contain small droplets of CeO_2 and Gd_2O_3 on the sub-nm scale,[7] even though the average structure remains fluorite and percolation theory can be used to rationalise the decrease of conductivity at larger concentrations. Nevertheless, the exact nature, structure and behaviour of extended defect clusters as a function of dopant concentration remains unclear. Similarly, a combination of Rietveld and Pair Distribution Function analysis on yttria-doped ceria has revealed[8] droplets of Y_2O_3 embedded in a ceria matrix even though the long-range structure is single phase. Our previous hybrid Monte Carlo simulations[4] on Gd-CeO_2 showed the formation of nanodomains of Gd_2O_3 even at low concentrations and molecular dynamics simulations on representative snapshot configurations produced by the Monte Carlo supported the hypothesis that such a network reduces ionic conductivity. A marked dependence of ionic conductivity on the dopant arrangement in rare-earth doped ceria and a prediction of long-term degradation in the system has also been made by means of a combination of DFT+U, parameterised Monte Carlo and kinetic Monte Carlo calculations by Grieshammer et al.[9]

In this paper we turn our attention to divalent dopants, in particular Ca^{2+} as well as the trivalent rare-earth element Gd. Calcium is cheaper than the rare-earths and its use preferable also on environmental grounds. When a divalent cation such as Ca^{2+} is incorporated into ceria, electroneutrality dictates that an oxygen vacancy is formed for each dopant cation,

$$CaO \xrightarrow{CeO_2} Ca''_{Ce} + V_O^{\cdot\cdot} + O_O^x \qquad (1a)$$

while with trivalent elements there is an oxygen vacancy for every two dopants:

$$Gd_2O_3 \xrightarrow{CeO_2} 2Gd'_{Ce} + V_O^{\cdot\cdot} + 3O_O^x \qquad (1b)$$

See ref. 4 for a brief discussion of available data for $Ce_{1-x}Gd_xO_{2-x/2}$. Lattice parameter variation for $Ce_{1-x}Ca_xO_{2-x}$ (CDC) with Ca^{2+} content have been reported by Arai et al.[10] and Thangadurai and Kopp[11]. The x-ray diffraction in the former study[10] indicate a cubic fluorite structure even up to $x = 0.8$, even though the authors assume a maximum solubility of CaO at $x = 0.23$. Measured conductivities fall slightly from $x = 0.1$ to 0.5 and then hugely thereafter. The authors in ref. 11 prepared samples in the range $x = 0$ - 0.25 both by co-precipitation and direct solid state high temperature reaction and noted similar lattice parameters. The transmission electron microscopy and x-ray photoelectron spectroscopy study of Yan et al.[12] over the range $x = 0.05$ - 0.5 has probed some of these issues further. At high Ca^{2+} concentrations the secondary phase present is face-centred cubic CaO and microdomains and superstructures are observed. With low-temperature sintering, $x = 0.1$ produces the highest ionic conductivity and the solubility limit is under 20% Ca. Conductivity is sensitive to preparation; for example, synthesis using different fuel-aided combustion reactions leads to different conductivities.[13] Conductivity maxima at $x = 0.1$ have also been observed by Shing et al.[14] and Yamashita et al.[15], while samples prepared by a mixed fuel process[16] showed a maximum at $x = 0.2$. Co-doping of CDC by the addition of Sm^{3+} or Gd^{3+} increases the ionic conductivity[17,18] to values larger than those for purely Sm^{3+} or Gd^{3+} doped ceria. Co-doping of CDC with Sr^{2+}also enhances the conductivity.[19] Molecular dynamics simulations[20] on ceria co-doped with two rare earths suggest that the conductivity of the co-doped lies within the range of the separate singly doped systems; these conclusions of course may not be

applicable to systems containing divalent cations. CaO also enhances grain-boundary conduction in gadolinia-doped ceria.[21] A calcium-doped ceria/sodium carbonate composite also exhibits higher ionic conductivity.[22]

There has been somewhat less attention paid computationally to $Ce_{1-x}Ca_xO_{2-x}$ than its rare-earth analogues. Calculations *in the dilute limit* and in the static limit (T = 0 K and neglecting all vibrations) suggest a preference for the divalent dopant and oxygen vacancy to be located at nearest neighbour positions and, as would be expected on electrostatic grounds alone, oxygen vacancies have larger association energies with divalent dopants than rare-earth trivalent cations.[23]

This paper reports results of Monte Carlo simulations of $Ce_{1-x}Gd_xO_{2-x/2}$ and of $Ce_{1-x}Ca_xO_{2-x}$ for a range of finite dopant concentrations x. These simulations do not use the hybrid Monte Carlo/molecular dynamics (HMC) method which we employed in ref. 4 for $Ce_{1-x}Gd_xO_{2-x/2}$, but a combined Monte Carlo/relaxation (MCR) technique discussed in more detail below in which it is more straightforward to trace vacancy positions. We are not restricted to the dilute limit in either HMC or MCR. Temperature effects are included; binding energies can strongly vary with T and clusters stable at low T can dissociate at higher temperatures. In addition, we make no constraints or assumptions, other than a simulation cell size of several thousand atoms, regarding local environments, and the configuration of Ca^{2+} and Ce^{4+} in the solid solution. Contact with experiment has previously been considerably restricted by assumptions required because of computational and methodological limitations.

Using a similar hybrid Monte Carlo approach to that in our previous work[4], Sun et al.[24] have shown that in rare-earth doped CeO_2 oxide ion diffusion is slower at edge dislocations because of the enrichment in rare-earth and depletion in mobile oxygen vacancies at these dislocations. By analogy with behaviour in metals, it had been suggested that dislocations also enhance ionic conductivity, but the reverse is observed in the simulations of Sun et al.[24] In this paper we also make a preliminary study of the Σ5(310) grain boundary in $Ce_{1-x}Gd_xO_{2-x/2}$ (x = 0.2) to examine if the same conclusion applies at a different type of interface.

2 Monte Carlo Simulations.

The properties of solid state materials, especially, ionic compounds, have traditionally been investigated using either supercell or point defect calculations.[25] These are not readily extendible to solid solutions with a finite dopant or defect concentration. Standard Monte Carlo (MC) and molecular dynamics (MD) is unable to overcome kinetic energy barriers to sufficiently sample all necessary configurations. In previous papers we have described MC methods that exchange cation positions in order to sample multiple configurations and calculate the thermodynamic and solubility limits of ionic materials.[26,27,28,29,30] MC simulations which *only* swap atoms will be very poor due to the different size and charge of the atoms, so that most swaps will be rejected and sampling of phase space will be poor. Thus some form of local relaxation is required since this can reduce enormously the energy required for any swap. We have developed a number of methods for this, including hybrid Monte Carlo/molecular dynamics (HMC).[19,26,28] This method allows us to include both the effects of atomic vibrations and relaxation, but it is not readily able to track the position of vacancies – at the high temperatures used in the molecular dynamics steps the highly mobile oxygens in this fast-ion conductor are assumed to adjust their positions. In addition, when the position of ions with significantly different charge (i.e. Ca^{2+} and Ce^{4+}) are exchanged it can be difficult to control the molecular dynamics simulation. In this paper we have used an alternative procedure, hybrid Monte Carlo/relaxation (MCR), in which the molecular dynamics simulation is replaced by a global optimisation (relaxation) of the atomic coordinates in the static limit. In contrast to the hybrid Monte Carlo/molecular dynamics, lattice vibrations are not included in the relaxation step itself although the position of vacancies can be monitored, as described in the next section.

Our method does not involve the use of an approximate parameterised Hamiltonian. Not only does parameterisation of, for example, an Ising-type Hamiltonian become increasingly difficult beyond binary or pseudobinary mixtures, but it can average out local effects due to ion clustering and association, and such methods cannot readily be extended to include the effects of lattice vibrations and pressure. The MCR technique permits an efficient sampling of different configurations and takes explicit account both of ionic relaxation near impurity ions and most thermal effects.

For consistency with previous calculations, the potential parameters used were those developed in ref. 23 (note that a different set of potentials for $Ce_{1-x}Gd_xO_{2-x/2}$ were employed in ref. 4). These authors have used these potential parameters extensively to study the ordering and clustering of divalent and trivalent dopants in ceria. Constraints on computational resources required us here to use rigid ions, rather than the shell model of ref. 23. The cutoff for the potentials was 20.0 Å. The potential parameters employed in our study are collected together in Table 1.

MC/Relax

In the MCR simulation at any stage one of two options is chosen at random, with equal probability. The first of these is an attempted random change in the volume of the cubic simulation cell, which is accepted or rejected using the standard Metropolis algorithm[31], such that a trial move from the original state (o) to a new state (n) is accepted with the probability,

$$P_{(o\rightarrow n)} = \exp\{-\beta[U_n - U_o]\} \qquad (2)$$

where U_n and U_o are the energies of the new and original states and β is $1/kT$. In the second, only applicable to the solid solution, a short static lattice minimisation follows exchange of randomly selected Ce and Ca ions or an oxygen ion and a vacancy. The energy minimisation was carried out using the FIRE method (Fast Inertial Relaxation Engine)[32] until either the maximum force was less than 0.001 eV/Å or the total energy was converged to within $1.0\text{x}10^{-5}$ eV. Again, the difference in energy between the previous configuration and that immediately after the relaxation is used in the Metropolis algorithm. If the exchange is rejected, the original configuration is included in the statistical averaging of thermodynamic properties and another swap then attempted. If accepted, the configuration is stored and the next cycle of the calculation proceeds from it.

As mentioned above the MCR technique does not include atomic vibrations in the relaxation step so in general in this step oxygen ions will not diffuse away in order to adapt their positions relative to those of the cations. It is essential that the positions of vacancies and oxygen anions are interchanged since the association energies between the vacancies and

Ca^{2+} ions are significant and can influence the sampling of configurations. It is not straightforward to track the location of vacancies (they are, after all, just empty space and in the relaxed structure formal assignment of a vacancy position is arbitrary). In our simulations the vacancies were treated as inert particles that were fixed in their positions during the relaxation step. Thus it is feasible to swap the position of a vacancy with an oxygen ion and the oxygens can move to the most energetically favourable position. Enthalpy and structural data were averaged over a period of 100,000 cycles, prior to which an equilibration period of 50,000 cycles was undertaken. Configurations were recorded every 1000 cycles and the length of the equilibration was determined by monitoring both the potential energy and the radial distribution functions of these configurations.

Molecular dynamics

In order to determine conductivities calculation of the ionic diffusion is required. This is not possible using our Monte Carlo technique and we turn to molecular dynamics simulations. Atomic configurations obtained from the Monte Carlo were used as starting points for the simulations. The MD simulations, with the DL_POLY code,[33] were undertaken in the isothermal-isobaric ensemble using Nosé-Hoover dynamics to control the temperature (1000 K) and pressure (1 atmosphere). The oxygen ion diffusion constant, *D*, is related from the mean squared displacements[34]:

$$6Dt(t \to \infty) = \langle r_i^2(t) \rangle = \frac{1}{N} \sum_{i=1}^{N} [r_i(t) - r_i(0)]^2 \qquad (3)$$

The ionic conductivity, σ, can then be obtained from the Nernst-Einstein relationship; while strictly valid for dilute systems only it is often used also for solid solutions:

$$\sigma_i = \frac{(z_i e)^2 cD}{k_B T} \qquad (4)$$

where $z_i e$ is the charge of species *i*, and *c* is the concentration of defects - here oxygen vacancies, which we assume is the only species responsible for the conductivity.

3. RESULTS

3.1 Structures

Figure 1 shows representative snapshots from MCR simulations of $Ce_{1-x}Gd_xO_{2-x/2}$. The MCR simulations of $Ce_{1-x}Gd_xO_{2-x/2}$ like the HMC simulations reported previously, used a cubic 8x8x8 simulation cell of CeO_2 containing the appropriate number of dopant cations and inert particles according to equation 1 (*e.g.* for x = 0.05 the number of Gd ions and inert particles/oxygen vacancies are 102 and 61 respectively). Thus all calculations were performed on simulation cells of 6144 ions with the Monte Carlo steps at 1000 K. Runs were undertaken on simulation cells ranging in composition from x = 0.0 to x = 0.4. Ref. 4 compares Monte Carlo simulations for end-members CeO_2 and Gd_2O_3 themselves. Both experimental and MCR calculated lattice parameters for the solid solution, like the HMC, exhibit a strong positive deviation from Vegard's law.

The structures and cation distributions in Figure 1 are also very similar to those from the HMC results presented in ref. 4 where a detailed analysis of bond lengths and local environments is given, and so this analysis is not repeated here. Calculated cation-cation radial distribution functions support the interpretation of power diffraction data using Pair Distribution Functions (rather than a more standard Rietveld analysis).[6] Several authors have postulated that the ionic conductivity is related to the trapping of vacancies around clusters of Gd^{3+} defects.[35] The picture which emerges from our structural analysis which includes the examination of local cation environments using order parameters is that an alternative description is the formation of nanodomains with the Gd_2O_3 structure. Thus at higher concentrations the overall mobility of oxygen vacancies decreases and diffusion paths are restricted, in broad agreement with the predictions of percolation theory for a cubic lattice.[7]

Figure 2 shows similar snapshots of the structures from MCR for $Ce_{1-x}Ca_xO_{2-x}$. Again all calculations were performed on simulation cells of 6144 ions with Monte Carlo steps at 1000 K. The clustering of Ca^{2+} is very pronounced even for the lower concentrations (x=0.1) in contrast to that in the plots for the Gd-doped system in Figure 1. Nanodomain 'droplets' of CaO tend to form lamellae that are perpendicular to [100]. The interface between the Ce and Ca rich regions is highly distorted.

3.2 Conductivities

Previous experimental and theoretical research, as discussed in the introduction, has identified a complex relationship between the atomic configuration and the ionic conductivity and the formation of domains reduces the ionic conductivity. To test this hypothesis and the influence of domains on the ionic conductivity, we have undertaken MD simulations, as described in section 2.3, using three different cation configurations as starting points for the simulations. We first consider the *random* distribution of cations. Both CDC and GDC have a maximum at x_{Ca} and x_{Gd} around 0.2. The conductivity for CDC is approximately double than that for GDC, which reflects the number of vacancies. The calculated conductivity of GDC is very similar to experiment. The conductivities associated with configurations *generated by the MCR* – the thermodynamically more stable configurations – are very low. For CDC the conductivity for such MCR configurations increases slightly from x_{Ca} = 0.2 to x_{Ca} = 0.3 which could possibly be attributed to distortions at the interface or a variation in percolation channels. We note that the MCR values are much lower than the conductivities of the random configurations in which fewer associated vacancies, vacancy clusters and nanodomains are present. Despite the significant approximations in our calculations, our results suggest that the growth of Gd-rich and Ca-rich domains have significant impact on the conductivities of GDC and CDC respectively.

3.3 Grain Boundary

As a first step towards examining interfaces and grain boundaries in particular, we have also run MCR simulations on the Σ5(310) grain boundary of $Ce_{1-x}Gd_xO_{2-x/2}$ where x_{Gd} = 0.10. Figure 5 displays a snapshot of the grain boundary and demonstrates the almost total segregation of the Gd^{3+} ions to the interface. Subsequently we have used molecular dynamics to determine the conductivity. The resulting conductivity is 0.016 S cm^{-1} which is about the same as the bulk MCR value and less than that for a random distribution of cations. Sun et al.[36] have shown that in rare-earth doped CeO_2 oxide ion diffusion is slower at edge dislocations because of the enrichment in rare-earth and depletion in oxygen mobility. Seeing no marked conductivity enhancement, our results are broadly similar to these results – in general there will be a play-off between the rare-earth enrichment and a possible reduction in

activation energies for migration mechanisms at interfaces, as is observed in metals and at the {001} surface of alkaline earth oxides.[37,38]

4. CONCLUSIONS

Monte Carlo calculations have been performed to examine the *thermodynamic equilibrium* properties of Gd-doped and Ca-doped ceria and on the Σ5(310) grain boundary of $Ce_{1-x}Gd_xO_{2-x/2}$. Our simulations include relaxation of the local environment around the different types of cation present in the solution and so provides efficient sampling of different configurations. These simulations do not take into account any kinetic factors, which are undoubtedly important in the fabrication of experimental samples and their behaviour over long time scales. The calculated conductivities of GDC and CDC suggest that experiments are undertaken on samples with a more random distribution of dopants i.e. not at thermodynamic equilibrium. Many experiments are unlikely to have been carried out under equilibrium because of the very long annealing times necessary. Aging processes which move the system towards thermodynamic equilibrium will thus lead to a marked decrease in conductivities.

CDC possesses even more pronounced domains than GDC with considerable distortion at the interfaces with the CaO nanodomains and the thermodynamically stable configurations again have low conductivities relative to those of randomly generated arrangements. In this context it is interesting that the calculated conductivities of random CDC configurations exceeds those of the randomly generated GDC analogues, although experimentally measured conductivities are lower. This might suggest a more pronounced tendency towards thermodynamic equilibrium in CDC, with lower kinetic barriers to segregation to nanodomains accompanying higher association energies between Ca^{2+} and oxygen vacancies.

5. Acknowledgements.

The SCARF computing resources were provided by STFC's e-Science facility. DSDG is funded by the EPSRC grant EP/K0162888/1.

Table

Species	*A* (eV)	ρ (Å)	C (eV Å^{-6})
Ce^{4+} - O^{2-}	1986.80	0.3511	20.40
Ca^{2+} - O^{2-}	784.38	0.3636	0.0
Gd^{3+} - O^{2-}	1885.75	0.3399	20.34
O^{2-} - O^{2-}	22764.3	0.1490	45.83

Table 1. The interatomic potentials from reference 23 which were employed in this study. *A,* ρ and *C* are constants used in the Buckingham potential which takes the form $\Phi_{ij} = A\exp(-r_{ij}/\rho) - Cr_{ij}^{-6}$

Figures

Figure 1

a

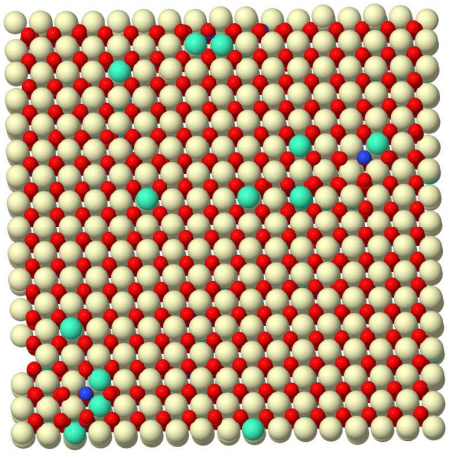

Jmol

b

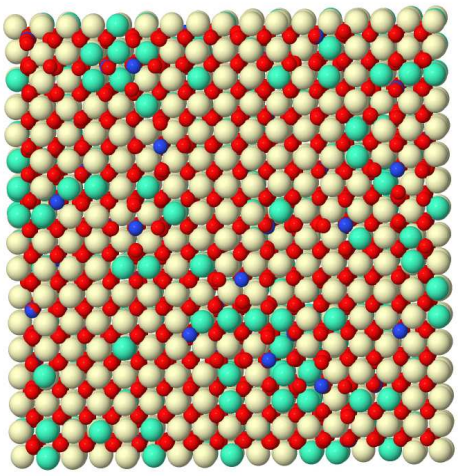

c

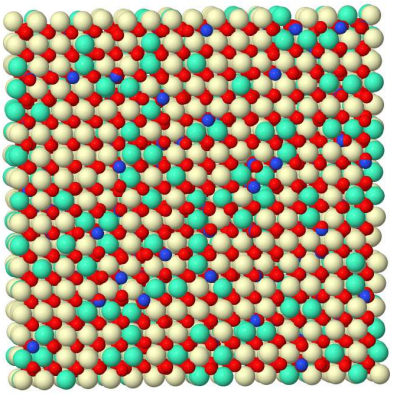

Figure 1. Gadolinium doped ceria for Gd^{3+} mole fractions x (a) $x = 0.05$, (b) $x = 0.10$ and (c) $x = 0.20$. Oxygens are red, cerium light brown, gadolinium light blue and vacancies dark blue.

Figure 2

a

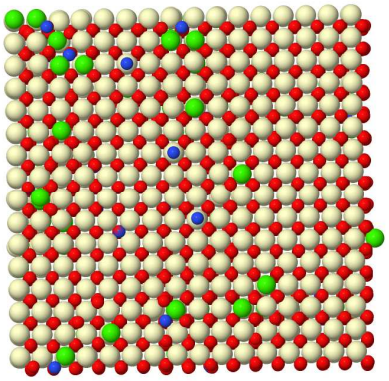

Jmol

b

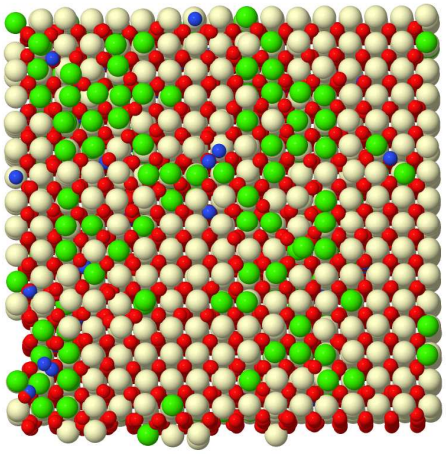

Jmol

c

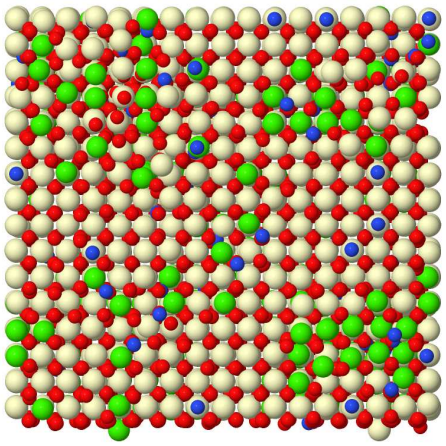

Jmol

d

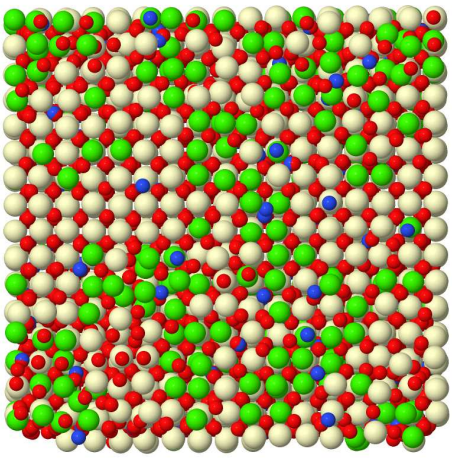

Jmol

e

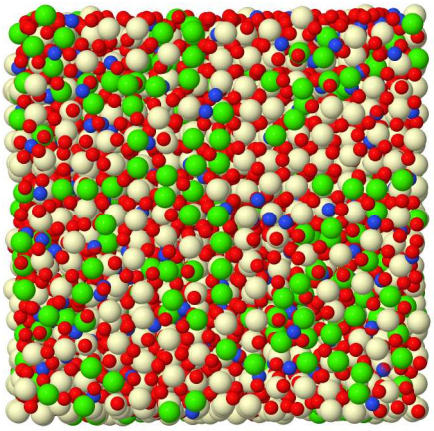

f

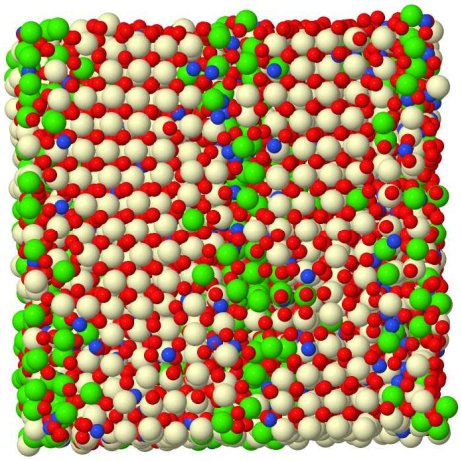

Figure 2. Calcium-doped ceria. (a) x = 0.05, (b) = 0.10, (c) x= 0.15, (d) 0.20, (e) 0.30 looking down [010] and (f) 0.30 looking down [100]. Colour scheme as figure 1, except that Ca is green.

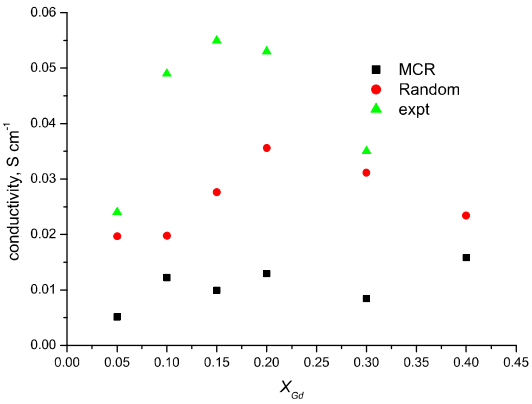

Figure 3. Ionic conductivities of Gd doped ceria calculated from molecular dynamics simulations of particular configurations. Circles are results obtained for the random distribution of Gd ions, whilst squares are configurations from the MCR simulations. The experimental values are taken from reference 39.

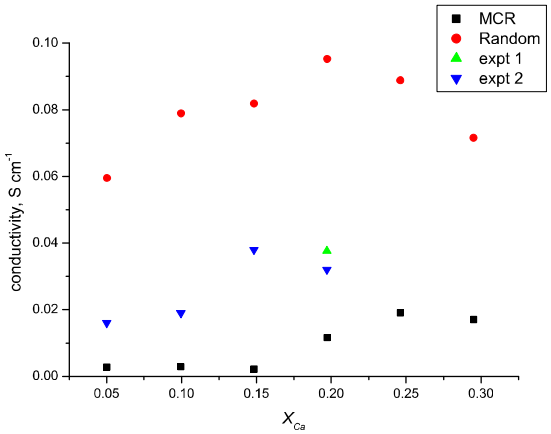

Figure 4. Ionic conductivities of Ca doped ceria. Circles are for configurations with a random distribution of Ca ions, whilst squares are results of molecular dynamics simulations on configurations obtained from the MCR simulations. Expt 1 and expt 2 refer to the experimentally determined values of Ma *et al.*[22] and Banerjee and Devi[16] respectively.

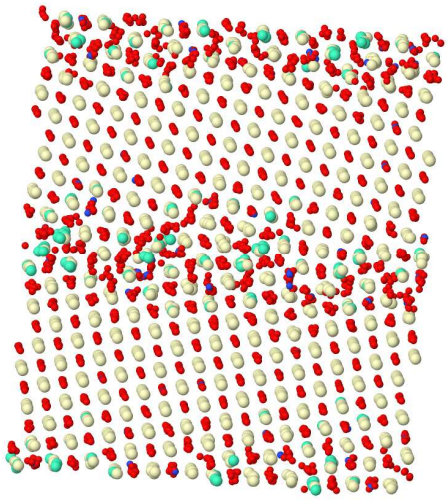

Figure 5. Σ5(310) grain boundary of GDC. Colour scheme as figure 1.

REFERENCES

[1] B.C.H. Steele, Solid State Ionics, 129 (2000) 95.

[2] B.C.H. Steele and A. Heinzel, Nature 414 (2001) 345

[3] J. Goodenough, Annu. Rev. Mater. Res. 33 (2003) 91.

[4] E.g., J. A. Purton, A. Archer, N.L. Allan and D.S.D. Gunn, J. Mater. Chem. A 4 (2016) 4592 and references therein

[5] T.S. Zhang, J. Ma, L.B. Kong, S.H. Chan and J.A. Kilner, Solid State Ionics, 209, **170**, 2004.

[6] M. Scavini, M. Coduri, M. Allieta, M. Brunelli and C. Ferrero, Chemistry of Materials, 24 (2012) 1338.

[7] M. Scavini, M. Coduri, M. Allieta, P. Masala, S. Cappelli, C. Oliva, M. Brunelli, F. Orsini and C. Ferrero, IUCrJ, 2 (2015), 511.

[8] M. Coduri, M. Scavini, M. Allieta, M. Brunelli and C. Ferrero, Chem. Mater. 25 (2013) 4278.

[9] S. Grieshammer, B.O.H. Grope, J. Koettgen and M. Martin, Phys. Chem. Chem. Phys. 16 (2014) 9974.

[10] H. Arai, K. Kunisaki, Y. Shimizu and T. Seiyaman, Solid State Ionics 20 (1986) 241

[11] V. Thangadurai and P. Kopp, J. Power Sources, 168 (2007) 178

[12] M. Yan, T. Mori, J. Zou, F. Yea, D.R. Ou, J. Drennan, Acta Materialia, 57 (2009) 722.

[13] P.S. Ong, Y.P. Tan, Y.H. Taufiq-Yapa and Z. Zainala, Materials Science and Engineering B 185 (2014)

[14] P.S. Ong, Y.P. Tan and Y.Y.H. Taufiq, Materials Science and Engineering 17 (2011) 012017

[15] K. Yamashita, K.V. Ramanujachary and M. Greenblatt Solid State Ionics 81 (1995) 53

[16] S. Banerjee and P.S. Devi. Solid State Ionics 179 (2008) 661

[17] S. Banerjee, K. Priolkar, and P. Sujatha Devi, Inorg. Chem., 50 (2011) 711

[18] X-Li. Zhao, J.-J. Liu, T. Xiao, J-C. Wang, Y-X. Zhang, H-C. Yao and J-S. Wang and Z-J. Li, J Electroceram 28 (2012) 149

[19] N. Jaiswal, D. Kumar, S. Upadhyay and O. Parkash, Ionics 20 (2014) 45

[20] M. Burbano, S. Nadin, D. Marrocchelli, M. Salanne, G.W.Watson, Phys. Chem. Chem. Phys., 16 (2014) 8320

[21] P-S Cho, S.B. Lee, Y.H. Cho, D-Y. Kim, H-M. Park, J-H. Lee, J. Power Sources, 183 (2008) 518

[22] Y. Ma, X. Wang, H.A. Khalifa, B. Zhu and M. Muhammed, Int. J. Hydrogen Ener., 37 (2012) 19401.

[23] Z.-P. Li, T. Mori, J. Zou and J. Drennan, Materials Research Bulletin, 48 (2013) 807

[24] L. Sun, D. Marrocchelli and B. Yildiz, Nature Comm. 6 (2015), 6294

[25] C.R.A. Catlow and W.C. Mackrodt, *Computer Simulation of Solids*; Springer-Verlag: Berlin, 1982.

[26] J.A. Purton, G. Barrera, N.L. Allan and J.D. Blundy, J. Phys. Chem. B, 102 (1998) 5202

[27] M.Y. Lavrentiev, N.L. Allan, G.D. Barrera and J.A. Purton, J. Phys. Chem. B, 105 (2001) 3594.

[28] J.A. Purton, N.L. Allan and J.D. Blundy, Chem. Comm., (1999) 707

[29] J.A. Purton, M.Y. Lavrentiev and N.L. Allan, J. Mater. Chem., 15 (2005) 785

[30] J.A. Purton, J.C. Crabtree and S.C. Parker, *Mol. Sim.*, 39 (2013) 1240

[31] N. Metropolis, A.W. Rosenbluth, M.N. Rosenbluth, A.H. Teller and E. Teller, J. Chem. Phys., 21 (1953) 1087

[32] E. Bitzek, P. Koskinen, F. Gähler, M. Moseler, and P. Gumbsch, Phys. Rev. Lett, 97 (2006) 170201

[33] W. Smith, T.R. Forrester and I.T. Todorov, *The DL_POLY Classic User Manual,* Daresbury Laboratory, 2010.

[34] M. Kilo, C. Argirusis, G. Borchardt and R.A. Jackson, Phys. Chem. Chem. Phys., 5 (2003) 2219

[35] J.A. Kilner, *Faraday Discussions*, 134 (2007) 9.

[36] L. Sun, D. Marrocchelli and B. Yildiz, Nature Comm. 6 (2015) 6294

[37] D.J. Harris, J.H. Harding, M. Lavrentiev, N.L. Allan and J.A. Purton, J. Phys.: Condens. Matter 16 (2004) L187

[38] G. Henkelman, B.P. Uberuaga, D.J. Harris, J.H. Harding and N.L. Allan, Phys. Rev. B. 72 (2005) 115437

[39] S. Zha, C. Xui and G. Meng J. Power Sources 115 (2003) 44.